Lawrence Berkeley Laboratory
UNIVERSITY OF CALIFORNIA

Presented at the International Conference
on ECR Ion Sources and Their Applications,
East Lansing, MI, November 16–18, 1987

Emittance Measurements on the LBL ECR Source

D.J. Clark

November 1987

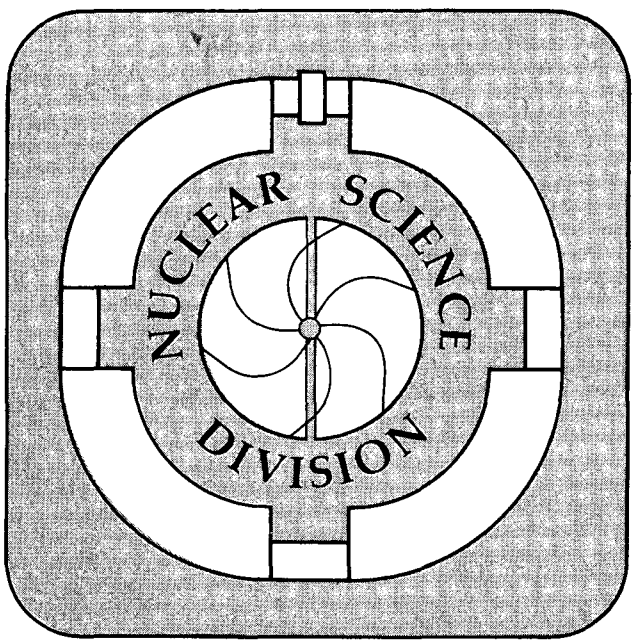

Prepared for the U.S. Department of Energy under Contract DE-AC03-76SF00098

DISCLAIMER

LBL 23866

EMITTANCE MEASUREMENTS ON THE LBL ECR SOURCE*

D. J. Clark
Lawrence Berkeley Laboratory, University of California
1 Cyclotron Road, Berkeley, CA 94720, U.S.A.

*This work was supported by the Director, Office of Energy Research, Division of Nuclear Physics of the Office of High Energy and Nuclear Physics and by Nuclear Sciences of the Basic Energy Sciences Program of the U.S. Department of Energy under Contract DE ACO3-76SF00098.

EMITTANCE MEASUREMENTS ON THE LBL ECR SOURCE

D. J. Clark
Lawrence Berkeley Laboratory, University of California
1 Cyclotron Road, Berkeley, CA 94720, U.S.A.

Summary. Measurements of radial emittance and the upper limit of energy spread have been made using a scanning Faraday cup after a waist, on beams of oxygen, argon and krypton. The general features are that the divergence seen at the scanning cup shows a central core and tails on each side. The un-normalized emittance of the beam core decreases with increasing Q/A in a way that is not explained by simple assumptions about the plasma or extraction system. Data from an experimental 1 mm diameter extraction aperture indicates that plasma density is about the same as over the standard aperture, but that the plasma energy spread is reduced to an upper limit of .2-.4 V, and beam brightness is up by a factor of 10 for medium charge states.

Introduction

The LBL ECR source and injection system have been described in previous papers (1), (2), (3) and in another paper at this Conference (4). This paper describes the use of a scanning Faraday cup to obtain plots of the beam width after an analyzing slit. This width is proportional to the beam divergence from the waist formed at the analyzing slit. Looking upstream, the divergence gives information about the beam formation in the source, including an upper limit of the energy spread in the source. Looking downstream, the divergence can be used together with the analyzing slit width to estimate the emittance of the beam which enters the injection system of the cyclotron.

Analyzing System and Scan Cup

The layout of the ECR source, and analyzing system is shown in Fig. 1. The source normally operates at +10 kV and the puller at -5 kV, using an accel-decel system. The source has an 8 mm diameter exit aperture. The source-puller distance is typically 3 cm. A Glaser magnetic solenoid lens focuses the beam on the object slit for the analyzing system, Slit 1, which is normally set at 1.3 cm width by 2.5 cm height.

The 90 degree analyzing magnet, designed by Y. Jongen, is approximately double focusing, with edge angles of 26.6 degrees. The effective angle for vertical focusing is reduced to about 23 degrees, due to the fringing field, so the vertical waist after the analyzing magnet is downstream

about 30 cm from the horizontal waist. The horizontal waist is at Slit 2, which is normally set at 1.3 cm width by 2.5 cm height, the same as Slit 1. A typical oxygen charge state spectrum is shown in Fig. 2. The magnet with the slit widths decribed above is sufficient to separate easily all the lighter heavy ion charge states. To separate isotopes of xenon the slit widths are sometimes reduced. There is some vertical loss of beam (10-20%) at the analyzing magnet for the lower charge states, making the spectrum appear more peaked toward higher charge states.

Faraday cups FC1 and FC2 are located after the slits. FC2 is suppressed for secondary electrons but FC1 is not. The first quadrupole in the injection system is shown in Fig. 1. It is turned off for the scan cup measurements to be described here. Several sets of beam centering magnets are located before and after the analyzing magnet.

The scan cup is located after the quadrupole, 213 cm downstream from Slit 2. This long drift distance makes possible the measurement of beam divergence at full intensity from the normal full width analyzing slit, rather than using a system which blocks most of the beam, such as set of narrow slits or holes, or a narrow scanning slit to break the beam up into beamlets. The cup consists of a current collector plate inside an enclosed box, with electrostatic suppression plates to prevent loss of secondary electrons from the plate. The beam current entering the box is defined by an entrance slit 1.6 mm wide by 13 cm high. The slit height is sufficient to transmit all the beam accepted by the 90 degree analyzing magnet aperture. The horizontal sweep distance is more than the full 15 cm width of the beam pipe. The cup is driven by a motor and lead screw through a bellows vacuum seal. The time for a 15 cm scan is about 1 minute. Scan data is taken on an X-Y recorder. This system has the advantage of good resolution and permanent recording, but for faster data collection a scanning wire or harp would be desirable.

Other devices shown on the beamline in Fig. 1 are an attenuator and a divergence collimator. The attenuator has a set of air driven meshes which can reduce the beam intensity without changing the emittance. The divergence collimator is a 4-jaw collimator with blades which can be swung into the beam to limit the divergence for beam diagnostic studies.

Scan Cup Measurements

Scan cup measurements were made of the charge states of several ion species, and with various source tuning conditions. In each case the beam was maximized on FC2. Two basic kinds of scans were done: 1) each charge state optimized for maximum current on FC2 using all source and transport parameters and 2) plasma conditions kept constant for all charge states, typically after tuning for a high charge state, with only the Glaser and analyzing magnets tuned to bring the beam to FC2. Type 1) scan is useful to study the emittance of each charge state as it would be optimized for injection into the cyclotron, and would appear on a beam list. Type 2) can be used to study some properties of the ECR plasma, extraction system and initial transport system under constant source conditions.

An example of type 1) measurement is shown in Fig. 3. Several charge states of oxygen from $O^{2+..7+}$ are displayed. On the horizontal axis is scan cup position as the cup moves across the beam pipe, converted to beam divergence, assuming that the beam originates in a waist at Slit 2. The vertical axis shows the beam current to the scan cup on a relative scale. The currents at FC2 are listed for each charge state. The source is tuned for each charge state, using source parameters such as magnet currents, RF power and gas flow. The high charge states optimize at lower gas flow and higher second stage magnetic field. There was less than 10% C^{3+} in the O^{4+} peak and no helium gas added for this run. Up to 15% of the FC2 beam is missing from the tails in these scan cup measurements, but the first quadrupole in the transport system accepts approximately the full FC2 beam.

Several features are apparent from the plots. They show a central low divergence core and high divergence tails for each charge state. The outer part of the tail falls outside the beam pipe. Also the core becomes narrower at high charge states, as would be expected from their higher energy.

In Fig. 4 is shown a similar plot for argon, with sample charge states from $Ar^{4+..13+}$. Oxygen is used as a mixing gas here but does not overlap with any of the argon charge states shown. The plots show the same kinds of core and tails and narrowing of the core at higher charge states as seen with the oxygen.

The emittance areas for the oxygen and argon beams above can be estimated for the total beam, including tails, and for the core of the beam. The results are summarized in Table 1. The areas are found by other experimental tests` to be approximately rectangular rather than elliptical. Both the rectangular areas and the areas of the surrounding ellipses are given. The width of the missing ends of the tails is estimated for the calculation. The cause of the tails could be a high energy group of ions in the plasma, a non-uniform region of the plasma meniscus at the source exit, or a non-linearity in the extraction system. The emittances are un-normalized, since the beam is transported at this energy and the transport program uses un-normalized emittance. Emittance in the vertical plane can be assumed to be the same, due to rotational symmetry at the source, except that there is some loss of the tails of low charge state beam at the analyzing magnet, and there is less focusing by the analyzing magnet. This was verified qualitatively by scans after rotation of the scan cup axis by 90 degrees. Other groups have made emittance measurements on ECR sources. At Grenoble (5) measurements were made on Micromafios, giving radial emittance areas of 90-460 π mm.mrad, un-normalized, for medium charge states of neon and argon at 7 kV source voltage. The GANIL group (6) finds emittance areas of a Minimafios source of 80-140 π mm.mrad, un-normalized, at 10-18 kV, for low and medium charge states of neon, argon and krypton. These are similar to the areas of the core beam in Table 1. In comparing emittances measured by various groups it would be useful to indicate, as these groups do, whether the area should be multiplied by π to obtain total area.

Type 2 scan cup measurements were also made, where the plasma was tuned for a high charge state and then plasma conditions were kept constant for scans of various charge states. This type of measurement can give information about the source plasma. An example is shown in Fig. 5, where the half-width at half maximum of the core of the beam is taken as a basic measure of the width. In Fig. 5 the plasma was first tuned for O^{7+}. Two runs are shown, taken two years apart, the first using helium as a mixing gas and the second with no helium. Intensities are higher in the second run. The points from the two runs are fairly consistent, with some scatter. The width clearly decreases with increasing charge state, Q, as it did in the Type 1 scans described above. A line proportional to an expected function of Q: $Q^{-1/2}$, is shown as a reference. This is discussed below.

Similar measurements for argon are shown in Fig. 6. Oxygen was used as a mixing gas, and contributes to the Ar^{5+} and Ar^{10+} but these are omitted on the plot. Here the plasma was first optimized for Ar^{8+}. The decrease in width with increasing charge state is seen again here.

Fig. 7 shows similar plots for krypton, with oxygen used as a mixing gas. The plasma was first optimized for Kr^{15+}. Both the krypton and oxygen widths are shown. The best grouping of the krypton and oxygen points was found when the horizontal axis was Q/A rather than Q, where A is atomic mass number. Again the width decreases with increasing charge state.

When running very light ions such as hydrogen and helium, the gas is fed into the second stage to get sufficient beam intensity, with the first stage turned off. Beam intensities of 200-300 eμA are obtained on FC2. In some cases an unsymmetrical scan pattern is obtained, such as shown in Figs. 8 and 9. Fig. 8 shows a proton scan with 2 different tunings of the plasma. The high intensity scan shows the beam peaked unsymmetrically about the 0 mrad center of the beam pipe. Fig. 9 shows a similar effect for He beams, but in this case with a constant plasma condition. It is surprising that the two plot symmetries are so different with the same plasma condition, although it is possible that the plasma condition changed between scans. This kind of assymmetry appears most often at the highest intensities, and may be due to plasma or exit meniscus conditions which are unsymmetrical across the axis.

An experiment to understand some of these effects was done by reducing the extraction aperture from 8 mm to 1 mm diameter. Two of the resulting scans on oxygen are shown in Fig. 10, overlayed on a standard scan for the 8 mm extractor. The beam intensities with the 1 mm aperture are reduced from the 8 mm aperture about proportional to the area, indicating that the plasma density is approximately constant over the area of the standard 8 mm extraction hole. The plots show that the divergence has become narrower for O^{7+} and much narrower for O^{4+} and that the tails have disappeared. A comparison with the rectangular emittances for the core beam of Table 1 for $O^{7+..4+}$ shows that emittance is a factor of 8 to 24 smaller, giving a brightness (α Current/Emittance^2) of a factor of about 1-10 times that of the core beam for the standard

8 mm extractor. The energy spread estimate is given below.

Interpretation of Results

The questions arising from the results above include:

1) What is the origin of the beam divergence, core and tails?
2) Why does the divergence have the measured dependence on Q and A?
3) What can we learn about the source energy spread?

One assumption about question 1) is that the divergence is due to the spread of ion velocities (or energies) in the source plasma perpendicular to the axis. The ion energy in the plasma $E_p \alpha Av^2$ or $v \alpha (E_p/A)^{1/2}$, where v is a typical ion velocity in the plasma. The velocity of the accelerated beam along the beam line, V, is given by the energy equation: $E_a = QV_s \alpha AV^2$, or $V \alpha (QV_s/A)^{1/2}$, where E_a is the energy of the accelerated beam and V_s is the source voltage. The divergence angle:

$\theta \alpha v/V \alpha (E_p/A)^{1/2} (QV_s/A)^{-1/2} \alpha (E_p/QV_s)^{1/2}$. The source voltage, V_s, is constant for all charge states. Since the plasma is very collisional we might assume that all charge states have the same energy, E_p. We then have the divergence $\theta \alpha Q^{-1/2}$. This dependence is shown in Figs. 5 and 6. The agreement is fair except for measurements above the curve in the medium charge states and below the curve for the highest charge states. But in Fig. 7 the best agreement between krypton and oxygen is found for a function like $(Q/A)^{-1/2}$ not $Q^{-1/2}$. This is true also for Figs. 5 and 6 where A is constant. So the assumptions made above of divergence being due to transverse ion energy spread in the plasma together with equal energies in the plasma for all ions does not fit the data for Fig. 7.

Another type of assumption is that divergence is due to ion energy spread in the plasma, as above, but that the ions are confined in a potential well, V_w, and they are lost when their energies rise above the well depth. Here calculations similar to those above lead to: $\theta \alpha (V_w/V_s)^{1/2}$ = constant, so all ions should have the same divergence. This also does not agree with the measurements.

Another contribution to source emittance is the rotational velocity given to the beam by the exit from the 3 kG magnetic field of the source to a zero field region. The conservation of canonical angular momentum tells us that the divergence, θ, of a beam with rigidity ($B\rho$) after

leaving a magnetic field, B, at a radius r from the axis is: $\theta = Br/[2(B\rho)]$. Since $(B\rho)$ is proportional to $(V_s\ A/Q)^{1/2}$ the dependence of this effect on Q and A is $\theta \alpha (Q/A)^{1/2}$, which also disagrees with the measurements. The emittance would be proportional to $r\theta$. The KVI group (7) finds that their ECR source emittance does have a $(Q/A)^{1/2}$ dependence, and so is strongly influenced by this effect. The Julich group (8) has also discussed this effect, and finds a strong effect upon the emittance, but this may be due to changing V_s rather than Q/A.

The scan cup measurements can also give an estimate of the energy spread of ions in the plasma, since the ion velocity transverse to the axis before extraction contributes to divergence of the beam after acceleration: $\theta \alpha\ v/V\ \alpha\ (E_p/A)^{1/2} / (E_a/A)^{1/2}\ \alpha\ (V_p/V_s)^{1/2}$, where V_p is the potential which would produce the ion energy spread in the plasma. Since other factors, such as meniscus aberrations and exit from the magnetic field, can also contribute transverse velocities, only an upper limit of plasma ion energies can be inferred, assuming a magnification of 1.5 from the source exit to slit 2. For the standard extraction aperture of 8 mm the half divergence angles (half of FWHM defined in Fig. 10) of scans of oxygen in Fig. 3 yield an upper limit of plasma ion voltage of .3 - 9 V for $O^{7+..1+}$. For the argon scans of Fig. 4 the upper limit is .4 - 6 V for $Ar^{13+..4+}$. For the 1 mm extraction aperture the upper limit of the energy spread is .2 - .4 V for $O^{7+..4+}$. It is likely that this very low voltage represents the true value of the plasma energy spread, since in this collisional plasma the ion energy probably doesn't vary over the 4 mm radius of the extraction hole. Power supply ripple makes a negligible contribution to this measurement, since the ripple would have to be 1% to give the measured spread on the scan cup, and power supply ripple has been measured to be a few parts in 10^4. This method of measuring the plasma energy spread has an advantage over measuring longitudinal energy spread with an analyzing system, because it can tolerate about 100 times more power supply ripple. The Grenoble group (9) has measured an energy spread of <1 V when using small extraction apertures.

Acknowledgements

The author wishes to thank C. Lyneis and W. Cooper for helpful discussions of material in this paper.

References.

1. C. M. Lyneis, "Operational Performance of the LBL 88-Inch Cyclotron with an ECR Source", Proc. 11th Int'l Conf. on Cyclotrons and their Applications, p. 707, Tokyo, Oct. 1986.

2. D.J. Clark and C.M. Lyneis, "Operation of the LBL ECR Source Injection System," Proc. 11th Int'l Conf. on Cyclotrons and their Applications, p. 499, Tokyo, Oct. 1986.

3. David J. Clark, "The LBL 88-Inch Cyclotron Operating with an ECR Source", Proc. Xth National Conference on Particle Accelerators", Dubna, Oct. 1986.

4. C. M. Lyneis, "Operating Experience with the LBL ECR source", this Conference.

5. N. Chan Tung, S. Dousson, R. Geller, B. Jacquot and M. Lieuvin, "Some Radial Emittance Measurements of the Multiply Charged Heavy Ion Source Micromafios", Nucl. Instr. & Meth. 174, 151 (1980).

6. E. Baron, L. Bex and M. P. Bourgarel, "Operation of the GANIL ECR Source", Proc. 7th Workshop on ECR Sources, p. 25, Julich, May 1986.

7. A. G. Drentje, "Half a Year Experience with the KVI-ECR Source", Proc. 5th E.C.R. Ion Sources Workshop, Louvain-la-Neuve, Apr. 1983.

8. W. Krauss-Vogt, "Some Aspects of Ion Extraction from ECR Sources", Proc. 7th Workshop on ECR Sources, p. 274, Julich, May 1986.

9. F. Bourg, P. Briand, J. Debernardi, R. Geller, B. Jacquot, P. Ludwig, M. Pontonnier and P. Sortais, Proc. 7th Workshop on ECR Sources, p. 187, Julich, May 1986.

Table 1. Emittance Measurements - Beam Optimized for Each Charge State

Ion	Emittance (high to low charge states)			
	Total beam including tails		Core only	
	Rectangular (mm.mrad)	Surrounding Ellipse (π mm.mrad)	Rectangular (mm.mrad)	Surrounding Ellipse (π mm.mrad)
$Oxygen^{7+..1+}$	1000-1600	500-800	90-500	50-250
$Argon^{13+..4+}$	800-1600	400-800	100-400	50-200

Notes: Total beam is beam on FC2.

Core only beam is beam within the full width at half maximum of the core. It contains 1/4 - 2/3 of FC2 beam, high to low charge states.

Acceleration voltage is 10 kV. Emittances are un-normalized.

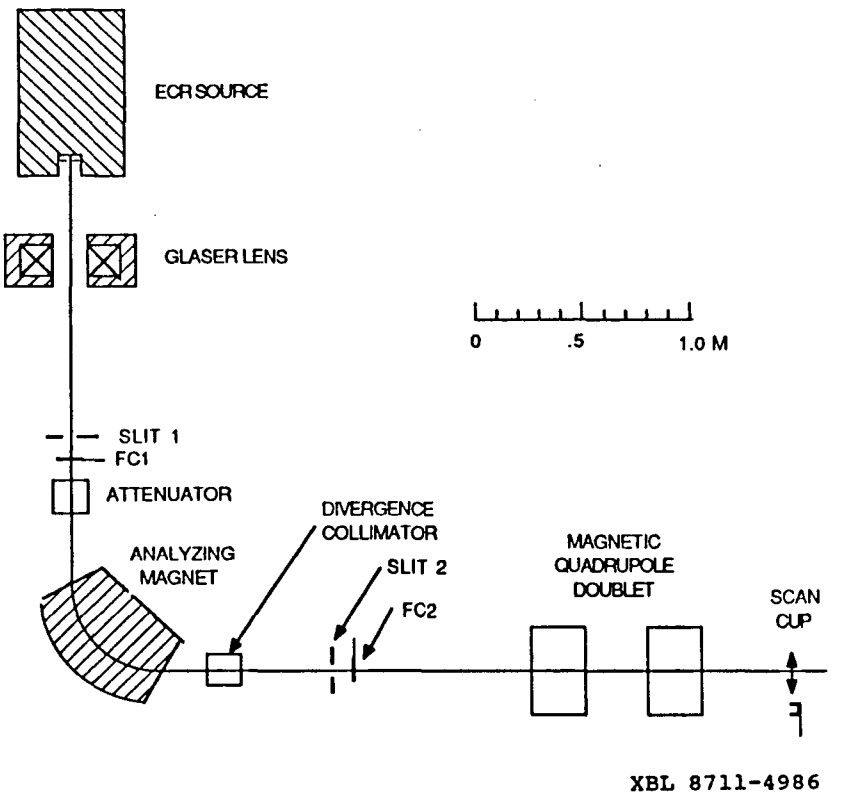

Fig. 1. Beam line from the ECR source to the scan cup.

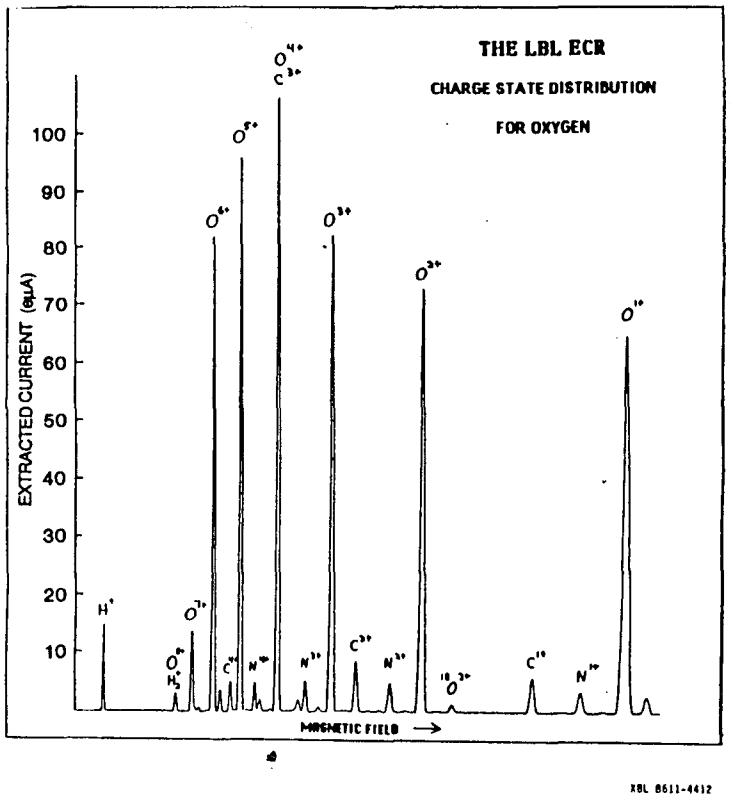

Fig. 2. Typical oxygen spectrum at FC2 after analyzing magnet, from X-Y recorder.

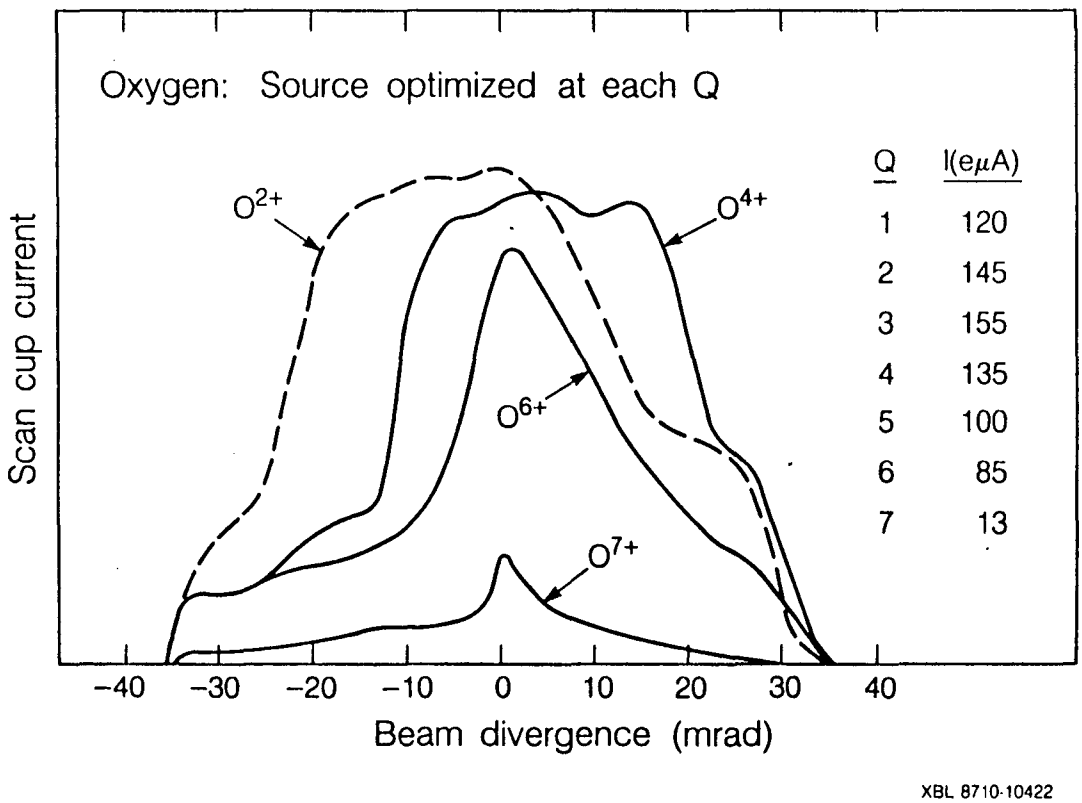

Fig. 3. Scan cup data for oxygen from X-Y recorder.

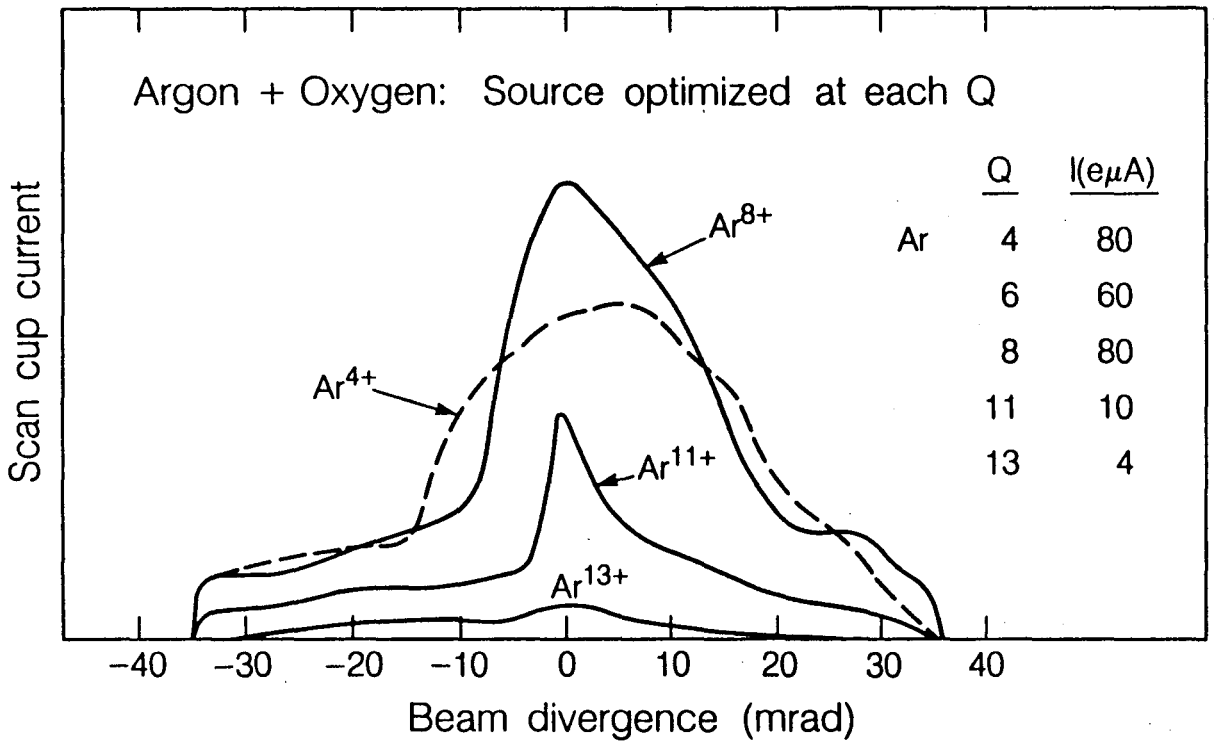

XBL 8710-10423

Fig. 4. Scan cup data for argon from X-Y recorder.

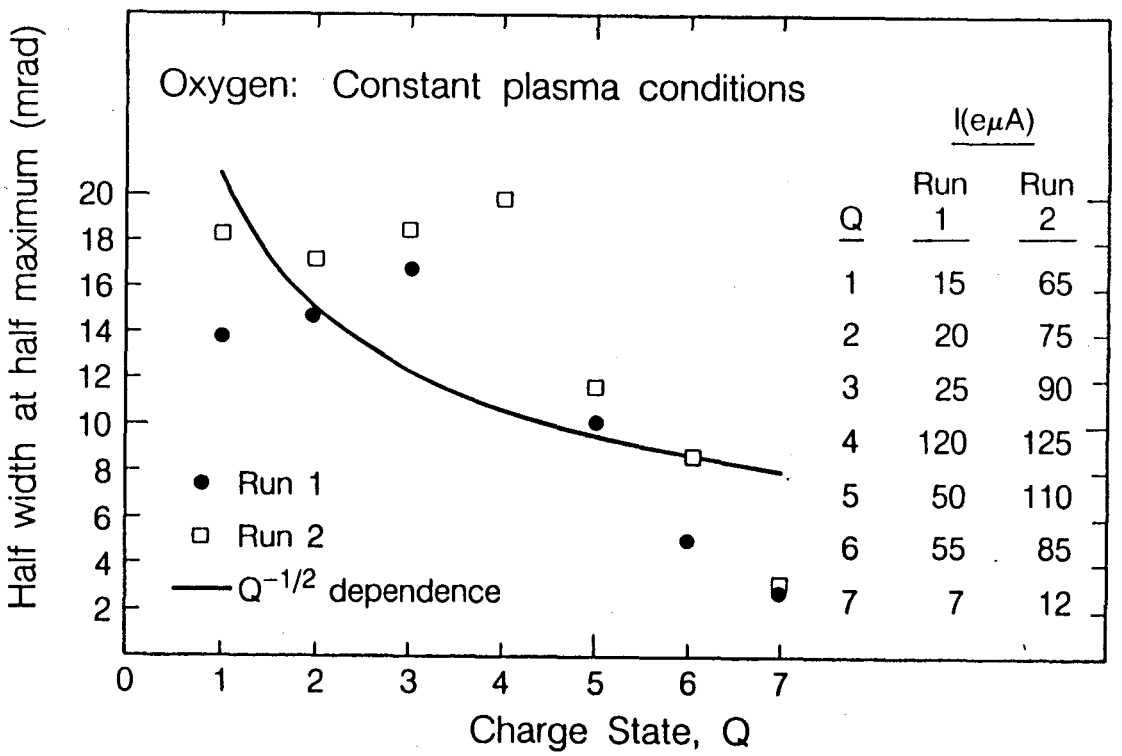

XBL 8710-10425

Fig. 5. Divergence vs. charge state for oxygen.

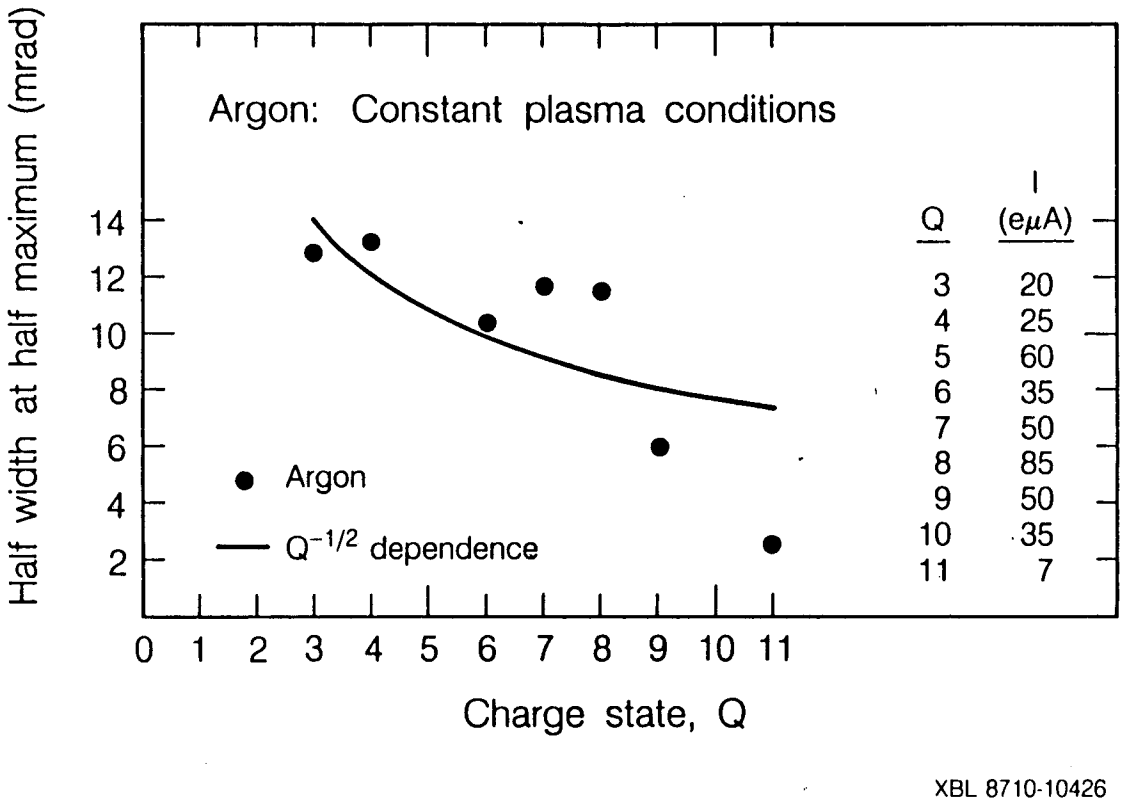

Fig. 6. Divergence vs. charge state for argon.

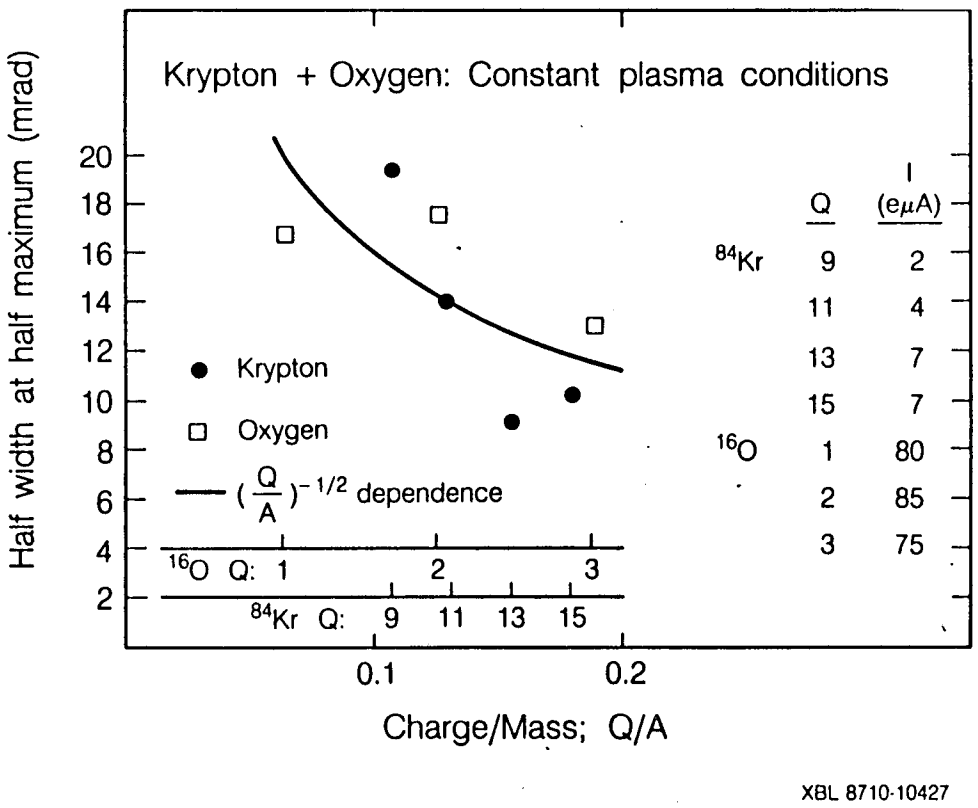

Fig. 7. Divergence vs. charge state for krypton and oxygen.

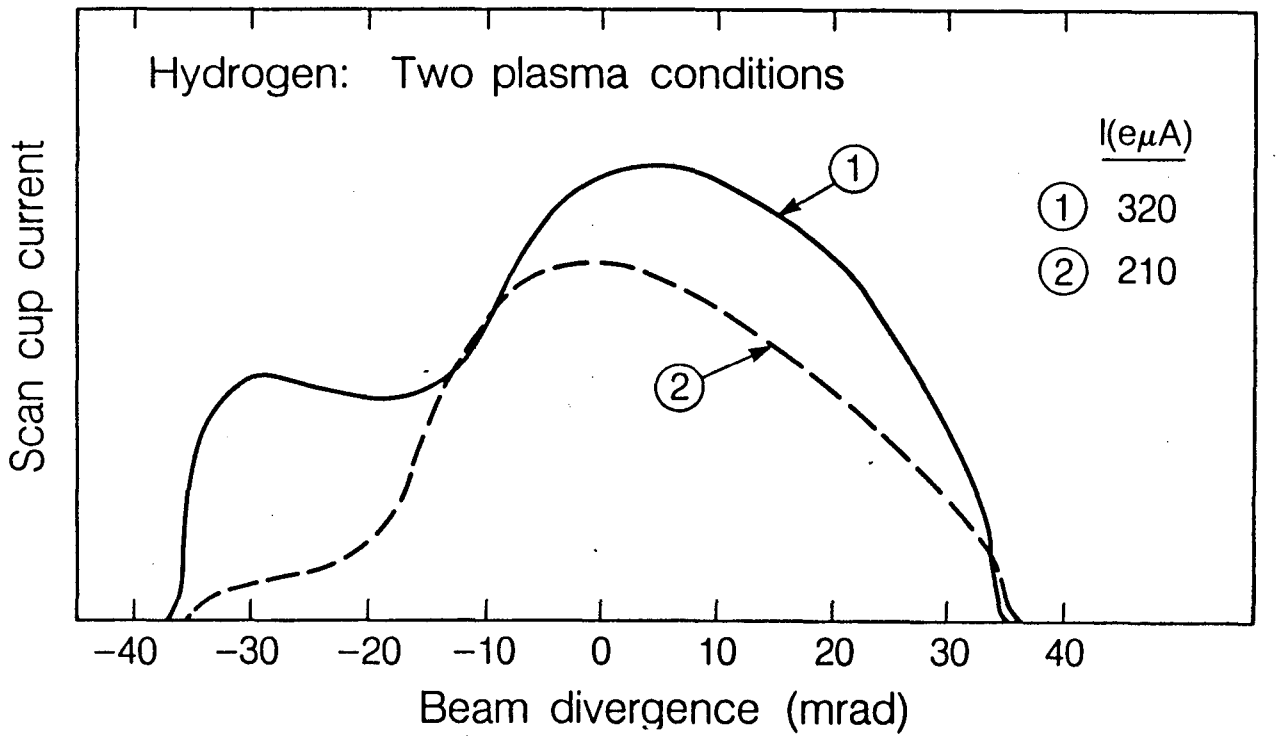

XBL 8710-10421

Fig. 8. Scan cup data for unsymmetrical proton beam from X-Y recorder.

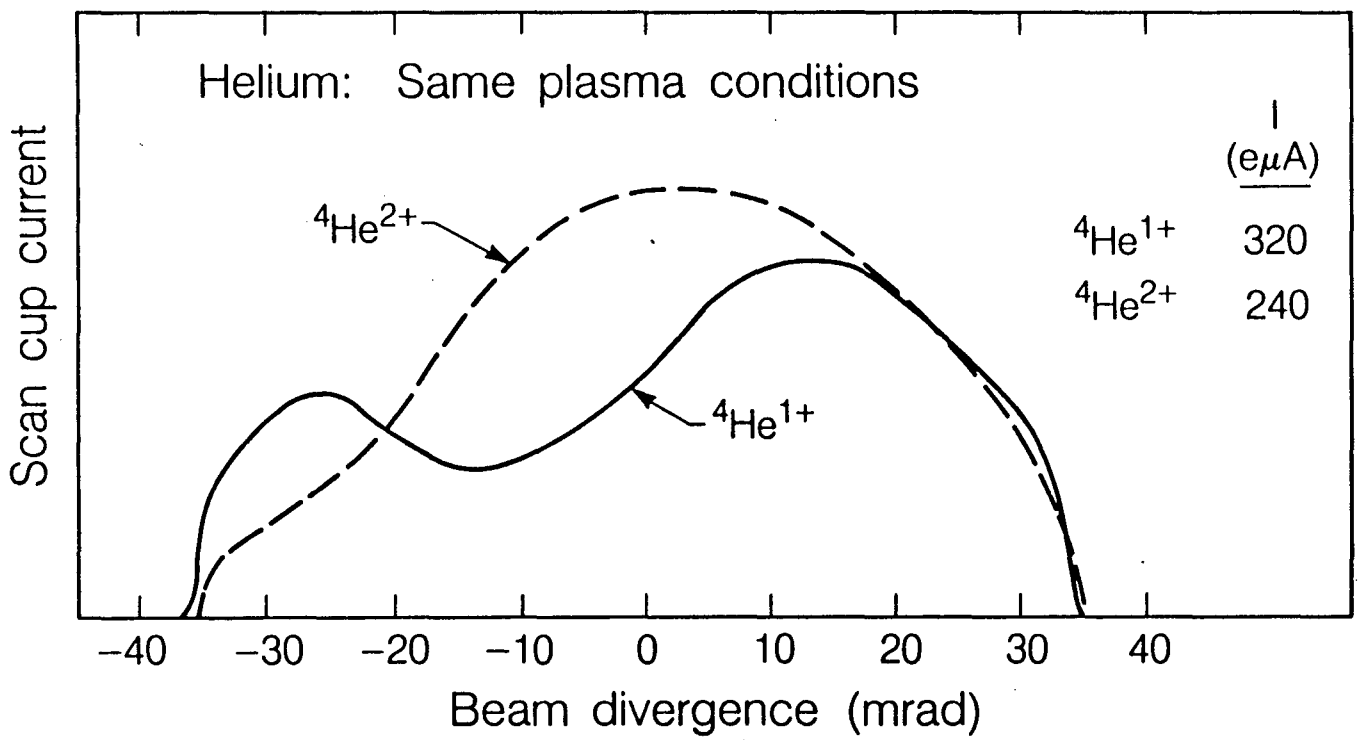

XBL 8710-10428

Fig. 9. Scan cup data for unsymmetrical helium beam from X-Y recorder.

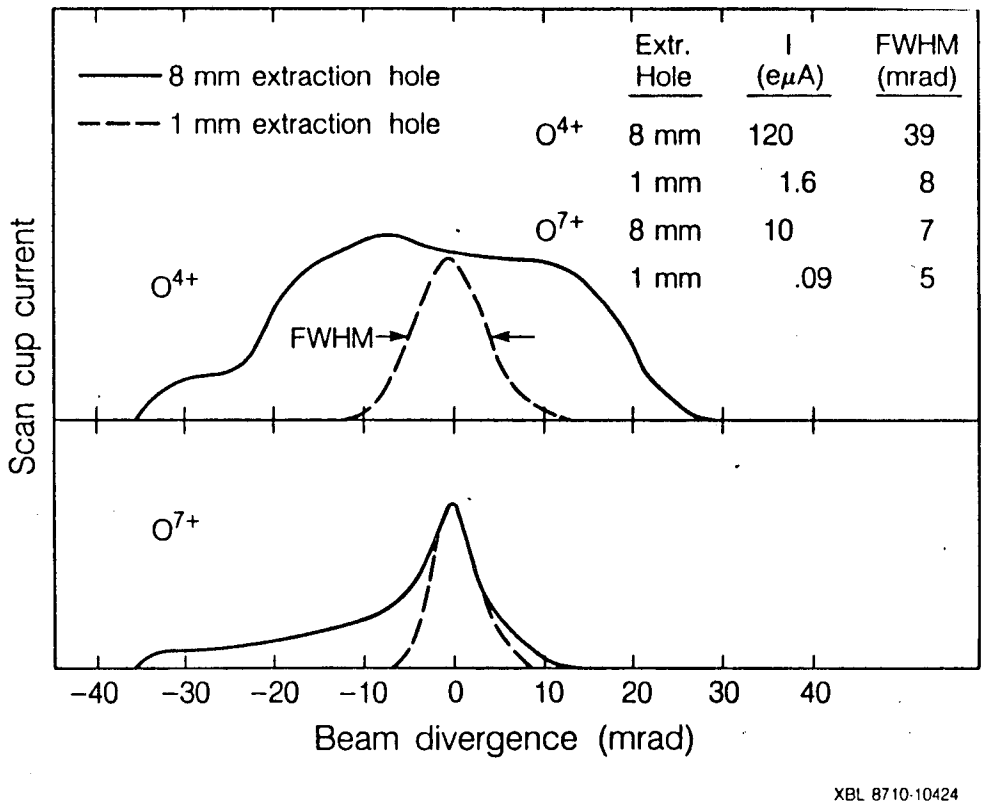

Fig. 10. Scan cup data for 1 mm and 8 mm extraction apertures from X-Y recorder.

LAWRENCE BERKELEY LABORATORY
TECHNICAL INFORMATION DEPARTMENT
UNIVERSITY OF CALIFORNIA
BERKELEY, CALIFORNIA 94720